Available online at www.dergipark.org.tr/en

INTERNATIONAL ADVANCED RESEARCHES and ENGINEERING JOURNAL

Journal homepage: www.dergipark.org.tr/en/pub/iarej

e-ISSN: 2618-575X

International Open Access

Volume 10
Issue 02

August, 2026

Research Article

Artificial intelligence-assisted performance prediction and operating-point identification for passive heat recovery ventilation systems

Hakan Tutumlu [a,*]

[a]*Department of Electrical and Energy, Naci Topcuoglu Vocational High School, Gaziantep University, 27630 Gaziantep, Türkiye*

ARTICLE INFO

Article history:
Received 20 April 2026
Accepted 22 August 2026
Published 25 August 2026

Keywords:
Carbon reduction
Cross-flow plate heat exchanger
Energy efficiency
Gradient boosting
Heat recovery ventilation
Indoor air quality
Machine learning
Passive ventilation
Random forest

ABSTRACT

Heat Recovery Ventilation (HRV) systems reduce building energy demand by thermally coupling exhaust and fresh outdoor air streams through a plate heat exchanger core, without auxiliary heating. This study presents a machine-learning (ML) framework for predicting and optimizing the passive performance of the Argemsan K-203 cross-flow plate heat exchanger under variable airflow conditions. Outdoor fresh air at 7.8°C/81%RH was drawn through the HRV core and supplied to the occupied space, while indoor exhaust air at 21.1°C /55%RH was simultaneously discharged outside through the same core-the built-in 1500W electrical heater was intentionally deactivated throughout. Experiments were conducted over 60 minutes at 13 measurement states spanning $u_t \in \{2, 4, 6\}$ m/s and $u_e \in \{2, 4, 6, 7.2\}$ m/s. Three regression models - Random Forest (RF), Gradient Boosting (GB), and Ridge Regression-were evaluated via Leave-One-Out Cross Validation (LOO-CV). RF achieved R^2 =0.931, MAE=0.261°C for fresh-air outlet temperature (T_4); Gradient Boosting achieved R^2=0.880 for sensible efficiency (η_T). Sensible efficiency ranged from 48.2% to 78.8% (mean 58.9%) and a humidity-ratio–based latent effectiveness of 35-59% (mean 44%). Recovered heat power spanned 245-713W, yielding 236-685 kWh/year of annual energy savings and 48-138 (natural gas) or 100-290 (grid) kgCO_2/year avoidance per unit. Response-surface analysis identifies u_t=2 m/s with $u_e \geq$6 m/s as the optimal operating band.

1. Introduction

The building sector accounts for approximately 36% of global final energy consumption and 39% of energy related CO_2 emissions [1]. The European Union's Energy Performance of Buildings Directive (EPBD) mandates near-zero-energy building (nZEB) targets for all new constructions [2]. Within HVAC systems, ventilation is a major energy sink: outdoor air must be conditioned to indoor comfort standards before delivery, and the thermal content of exhaust air is conventionally wasted. HRV systems address this by thermally coupling exhaust and supply streams through a heat exchanger core, recovering energy without auxiliary heating input [3].

In a passive HRV configuration-the focus of the present Study-heat transfer occurs entirely through conduction across aluminum plate surfaces, with no supplementary electrical or combustion heating. Thermal performance is conventionally characterized by a single rated efficiency obtained under EN 308 standard conditions [4]. In practice, performance varies strongly with the flow rates on both sides, ambient temperature and humidity, and seasonal climate variability [5-6]. Conventional fixed-efficiency models are therefore insufficient for real-time prediction and control.

ML models trained on in-situ sensor measurements can capture non-linear dependencies among operating variables without explicit knowledge of exchanger geometry [7-8]. Ensemble tree methods such as Random Forest and Gradient Boosting demonstrate strong predictive performance on small tabular datasets typical of building science experiments [9]. The present study employs the Argemsan K-203 training unit [10] and makes four contributions: (1) a structured experimental dataset from 12 passive-HRV operating conditions; (2) a systematic LOO-CV comparison of three ML models for T4 and η_T prediction; (3) a two dimensional response-surface optimization over the (u_e, u_t) velocity space; and (4) a quantified energy and carbon reduction analysis linking HRV efficiency to annual CO_2 avoidance under Gaziantep climate conditions.

* Corresponding author. Tel.: *+90 530 926 1175*; Fax: +90 342 337 1138.
E-mail addresses: htutumlu@gantep.edu.tr (H.Tutumlu)
ORCID: 0000-0003-3884-7015 (H.Tutumlu)
DOI: 10.35860/iarej.1934313
© 2026, The Author(s). This article is licensed under the CC BY-NC 4.0 International License (https://creativecommons.org/licenses/by-nc/4.0/).

2. Review of the Literature

2.1 HRV performance

Fanger (1970) and Persily & Emmerich (2012) define the thermal-comfort and IAQ constraints that bound acceptable T_4 values [11-12]. Persily (2016) established field-measurement protocols for ventilation systems and quantified the gap between rated and in-situ performance [13]. Nasif et al. (2010) demonstrated non-linear coupling between sensible and latent heat transfer in variable-air-volume systems [6]. Choi et al. (2018) showed that temperature efficiency can vary by up to 20 percentage points across seasonal climates [5]. Zhao and Liu (2022) further demonstrated that the feasibility and performance of heat recovery ventilation systems are strongly influenced by climate conditions and occupant behavior, highlighting the critical role of operational parameters in system optimization [14]. Recent air-to-air heat-recovery studies report cross-flow plate effectiveness in the 50–75% range [15] and provide directly comparable fixed-plate energy-recovery-ventilator [16] and combined mechanical-ventilation-heat-recovery/solar pre-heating [17] benchmarks; related HVAC thermal-performance analyses have also appeared in this journal [18]. More recent work reinforces these trends: Hamburg et al. [19] evaluated centralized and decentralized mechanical ventilation with heat recovery for the deep renovation of high-rise apartment buildings, while Amir et al. [20] experimentally quantified heat-pipe-based recovery effectiveness under varying fresh-air intake temperatures.

2.2 ML in buildings

Tsanas & Xifara (2012) applied RF to a 768-sample building energy dataset, achieving sub-2% normalized RMSE [21]. Aste et al. (2017) surveyed ML approaches for building energy and control, consistently recommending ensemble methods for small-N datasets [7]. Kallio, Johanna, et al.(2021) showed ensemble methods outperform linear models for indoor CO_2 and energy prediction using machine learning [22]. Demirezen, Gulsun, et al. (2020) trained neural networks for heat-exchanger performance, reporting R^2>0.95 for outlet temperature [23]. Wang et al. (2019) highlighted feature importance interpretability as critical for operational HVAC decision-making [24].

2.3 Carbon accounting

International Energy Agency (2023) reports Turkey's grid electricity emission factor at 0.423 $kgCO_2$/kWh [25]. IPCC (2006) assigns 0.202 $kgCO_2$/kWh for natural gas [26]. Bao et al. investigated the performance of heat recovery ventilation systems across five different climate regions and demonstrated that climatic conditions substantially influence their energy-saving potential, with greater heat recovery benefits observed in colder regions [27]. Menter et al. (2003) confirmed that SST k-ω turbulence modelling is consistent with duct velocity profiles at the K-203 geometry, supporting the mass-flow calculation in Section 3 [28].

3. Background of System Thermodynamics, AI, and Statistical Models

3.1 Passive HRV Operating Principle and Mass Flow

In the passive configuration studied here, fresh outdoor air (state: T_3, RH_3) enters one side of the cross-flow core, gains heat from the opposing exhaust stream, and is delivered to the space at T_4, RH_4. Indoor exhaust air (T_1, RH_1) gives up heat and is discharged at T_2, RH_2. The 1500W heater of the K-203 unit was intentionally deactivated; all heat exchange occurred exclusively through plate conduction.

With duct diameter d=0.15m and air density ρ = 1.2 kg/m^3:

$$\dot{V}_t = 0.785d^2 \cdot 0.9u_t \tag{1}$$

$$\dot{m}_t = \dot{V}_t \cdot \rho \tag{2}$$

The factor 0.9 corrects for the parabolic velocity profile (u=0.9·u_{max}) in circular ducts [28]. At u_t=2m/s: $\dot{m}_t$= 0.0382 kg/s; at u_t=6m/s: $\dot{m}_t$= 0.1145 kg/s.

3.2 Thermal Performance Metrics

The primary metric is the NTU-effectiveness:

$$\eta_T = \frac{T_4 - T_3}{T_1 - T_3} \times 100\% \tag{3}$$

This is bounded in [0, 100%] and independent of the flowrate ratio between the two streams [4]. The K-203 manual additionally defines the heat-balance efficiency [10]:

$$\eta_{K203} \cong \frac{T_4 - T_3}{T_1 - T_2} \times 100\% \tag{4}$$

Both metrics are computed and compared in Table 3. Moisture recovery efficiency:

$$\eta_{RH} = \frac{RH_4 - RH_3}{RH_1 - RH_3} \times 100\% \tag{5}$$

3.3 Recovered Heat Energy and Carbon Savings

Instantaneous useful heat energy:

$$\dot{Q}_{hrv} = \dot{m}_t c_p (T_4 - T_3) \quad [W] \tag{6}$$

with c_p = 1005 J/(kg·K). Annual energy savings (8 h/day, 120 heating days/year):

$$E_{saved} = \dot{Q}_{hrv}/1000 \times 960 \quad [kWh/year] \tag{7}$$

Annual CO_2 avoidance:

$$m_{CO_2} = E_{saved} \times EF \quad [kg/year] \tag{8}$$

where EF=0.202 kg/kWh (natural gas [26] or EF=0.423 kg/kWh [25].

3.4 Machine Learning Formulation

Feature vector $x_i = [T_1, T_3, RH_1, RH_3, u_t, u_e]^T \in \mathbb{R}6$, targets $y \in T_4, \eta_T$ }, N = 13. All features standardized to zero mean and unit variance. Model hyperparameters (RF: B=500 trees; GB: M=200 stages, ν=0.1) were kept at standard library defaults rather than tuned. With only N=13 samples, an explicit hyperparameter search would risk over-fitting the leave-one-out folds and inflating the apparent performance; the defaults therefore provide a deliberately conservative baseline. The three learners rest on established statistical-learning theory: Random Forest is a bagging ensemble of regression trees [29-30], Gradient Boosting builds additive tree expansions by stagewise steepest descent [31-32], and both are treated within the standard ensemble and statistical-learning framework [33-34]. Comparable small-sample, cross-validated regression pipelines have recently been reported for renewable-energy and thermal-storage prediction [35-36].

Random Forest (B = 500 trees):

$$\hat{y}_{RF}(x) = \frac{1}{B}\sum_{b=1}^{B} T_b(x) \tag{9}$$

Gradient Boosting (M = 200 stages, $\nu = 0.1$):

$$\hat{y}^{(m)}(x) = \hat{y}^{(m-1)}(x) + \nu\, h_m(x) \tag{10}$$

The LOO-CV evaluation metrics:

$$MAE = \frac{1}{N}\sum_i |y_i - \hat{y}_i| \tag{11}$$

$$RMSE = \sqrt{\frac{1}{N}\sum_i (y_i - \hat{y}_i)^2} \tag{12}$$

$$R^2 = 1 - \frac{\sum_i (y_i - \hat{y}_i)^2}{\sum_i (y_i - \bar{y}_i)^2} \tag{13}$$

$$\sigma_{MAE} = \frac{1}{\sqrt{N}} \cdot std(|e_i|) \tag{14}$$

4. Experimental Setup

4.1 Experimental Setup Unit - Argemsan K-203

All experiments used the Argemsan K-203 Heat Recover Local Ventilation Training Set [10]. The unit features a cross-flow aluminum plate heat exchanger, two independently controlled centrifugal fans (Fan 1: fresh-air supply; Fan 2: exhaust extraction), flexible ducts of inner diameter d=0.15 m, and a safety interlock (RCD + emergency stop). Fan speeds are set via phase speed control switches. The integrated 1500W electrical heater was not activated at any point; all thermal exchange occurred passively through the plate core. Sensor ports follow the K-203 designation: T_1/H_1 at exhaust inlet; T_2/H_2 at exhaust outlet; T_3/H_3 at fresh-air inlet; T_4/H_4 at fresh-air outlet. Each port has a calibrated combined temperature/RH transducer. Boundary conditions: outdoor dry-bulb 7.8°C, wet-bulb 9.4°C, *RH*81%; indoor dry-bulb 21.1°C, wet-bulb 15.0°C, *RH*55%. Figure 1 shows the physical experimental setup unit.

4.2 Measurement Protocol

Following the K203-02 thermal efficiency protocol [10], measurements were taken at 5-minute intervals over 60 minutes (N = 13; measurement 0: baseline, both fans off; measurements 1-12: active HRV). Steady state was confirmed before logging each point. Fan velocities followed a balanced partial-factorial design: $u_t \in \{0, 2, 4, 6\}$ m/s × $u_e \in \{0, 2, 4, 6, 7.2\}$ m/s. Table 1 provides the complete experimental dataset.

5. Results and Discussion

5.1 Experimental Profiles

Figure 2 shows temperature and humidity profiles. T_1 remained stable at 20.4-21.2°C (steady indoor conditions). Passive heat exchange raised T_4 to 15.1-18.3°C-a net gain of 4-8°C with zero auxiliary energy. η_T ranged from 48.2% to 78.8% (mean 58.9%; Table 1). Moisture recovery η_{RH} consistently exceeded η_T by 10-19 pp, consistent with the Lewis analogy for air/water-vapor systems [3].

However, because η_{RH} is defined on relative humidity, it is dominated by the temperature-driven RH shift rather than by genuine latent transfer. Re-evaluating moisture exchange on the humidity ratio w, obtained psychrometrically from the measured T and RH, gives a latent effectiveness of only 35-59% (mean 44%).

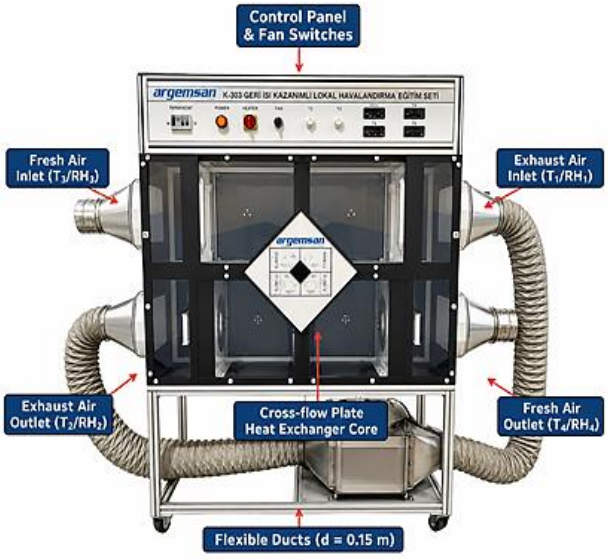


Figure 1. Heat recovery ventilation experimental setup

Table 1. Complete experimental dataset.

No.	t [min]	u_t [m/s]	u_e [m/s]	T_1 [°C]	T_2 [°C]	T_3 [°C]	T_4 [°C]	RH_1 [%]	RH_3 [%]	η_T [%]	η_{RH} [%]
0	0	0	0	21.2	18.3	11.3	17.3	58.4	74.5	60.6	84.5
1	5	2	2	21	18.3	11	17.4	58.7	76.1	64	88.5
2	10	2	4	20.7	18.3	10.8	18.1	58.2	77	73.7	95.2
3	15	2	6	20.7	18.7	10.6	18.3	58	77.7	76.2	97.5
4	20	2	7.2	20.4	18.4	10.5	18.3	58	78	78.8	98
5	25	4	2	21.2	17	11	16	57.3	79.1	49	63.8
6	30	4	4	21	17.2	9.5	15.1	57.3	80.5	48.7	65.1
7	35	4	6	21.2	17.7	9.7	16	56.5	80	54.8	72.3
8	40	4	7.2	20.8	17.3	9.4	15.6	56.7	80.4	54.4	72.2
9	45	6	2	20.7	16.2	9.7	15.4	57.1	80	51.8	59
10	50	6	4	21.1	17	9.7	15.2	56.4	80.1	48.2	62.9
11	55	6	6	20.8	17.2	9.4	15.6	56	81.3	54.4	67.2
12	60	6	7.2	21.2	17.6	9.4	15.6	55.4	80.9	52.5	67.1

The persistent $w_4 > w_3$ indicates a small inter-stream moisture gain, consistent with limited cross-leakage in the aluminium core rather than membrane-type latent recovery. Each condition was measured once and the velocity levels were applied sequentially, so the apparent ut sensitivity is partly confounded with a slow downward drift of the fresh-air inlet temperature T_3; replication and randomised ordering are needed to separate these effects. At u_t=2 m/s, increasing u_e from 2 to 7.2 m/s raised η_T by 14.8 pp (64.0%→78.8%). Increasing u_t from 2 to 6 m/s at constant u_e=6 m/s reduced η_T by 21.8 pp (76.2%→54.4%), because shorter residence time limits heat transfer. This asymmetric sensitivity-large negative effect of u_t, moderate positive effect of u_e-is the key operational finding.

5.2 Machine Learning Performance

Table 2 summarizes LOO-CV results. RF achieved R^2=0.931 (MAE=0.261±0.21°C, σ over 13 LOO folds) for T_4 prediction. Given N=13, these estimates carry substantial sampling uncertainty; bootstrap resampling (B=1000) over the LOO residuals yielded a 95% confidence interval of $R^2 \in [0.82, 0.96]$, indicating that the point estimate should be interpreted with caution [22]. For η_T , the three regressors perform comparably; the best fit is Gradient Boosting (R^2=0.880), with Random Forest and Ridge Regression close behind within the tested range. Random Forest attains comparable η_T accuracy (R^2=0.868), and no model shows the pronounced overfitting expected at this small sample size [22]. Figure 3 presents predicted vs. measured T_4 for all three models (panel a), error metrics (panel b), and RF Gini feature importance (panel c). The supply velocity u_t ranks first, followed by the inlet humidities RH_3 and RH_1, consistent with the dominant role of u_t identified in the velocity analysis; the inlet temperatures T_3 and T_1 and the exhaust velocity u_e contribute least. Because most of the predictive signal is carried by u_t and the two inlet humidities, a reduced-instrumentation set is proposed only as a hypothesis for future work [23].

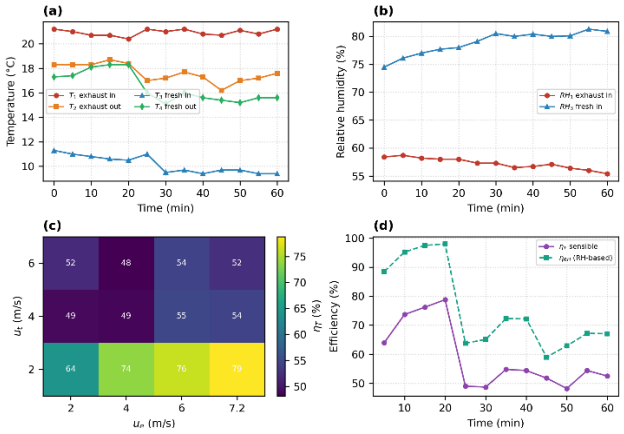


Figure 2. Measured profiles (passive HRV). (a) Temperatures; (b) relative humidities; (c) η_T map; (d) efficiency time series.

Table 2. LOO-CV prediction performance

Target	Model	MAE	RMSE	R^2
T_4 (°C)	**Random Forest**	**0.261±σ₁**	**0.311±σ₁**	**0.931**
	Gradient Boosting	0.292±σ₂	0.349±σ₂	0.913
	Ridge Regression	0.344±σ₃	0.421±σ₃	0.874
η_T (%)	Random Forest	3.290±σ₄	3.937±σ₄	0.868
	Gradient Boosting	2.870±σ₅	3.746±σ₅	0.880
	Ridge Regression	**3.491±σ₆**	**4.281±σ₆**	**0.844**

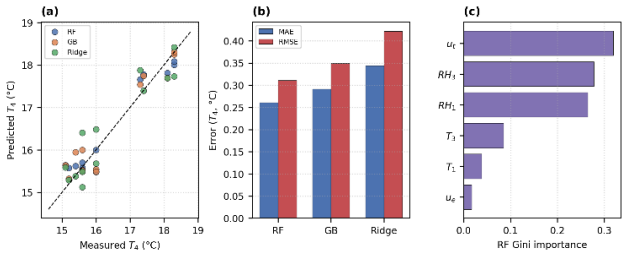


Figure 3. LOO-CV evaluation. (a) Predicted vs. measured T_4; (b) error metrics; (c) RF feature importance.

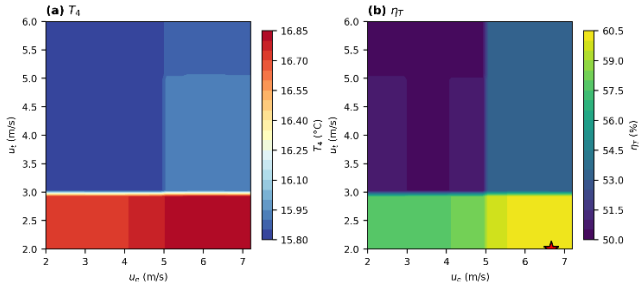


Figure 4. RF response surfaces over (u_e, u_t); (a) T_4; (b) η_T with optimum (⋆) at u_e ≈6.7, u_t =2.0 m/s

5.3 Response Surface Optimization

Figure 4 shows RF response surfaces for T_4 (panel a) and η_T (panel b) over the (u_e, u_t) plane (other features held at experimental means: T_1=21.0°C, T_3=9.9°C, RH_1 = 56.9%, RH_3 = 79.5%). The η_T surface peaks at u_e≈6.7 m/s, u_t=2.0 m/s, with η_T≈60.1% and T_4≈16.5°C. The contour gradient is substantially steeper in the u_t direction than in u_e, quantitatively confirming the asymmetric sensitivity in Section 5.1.

Table 3. Efficiency metric comparison: NTU-effectiveness vs. K-203 heat-balance ratio for all active operating conditions.

No.	u_t [m/s]	u_e [m/s]	η_T NTU [%]	η_{K203} Heat-bal. [%]
1	2	2	64	95
2	2	4	73.7	87.8
3	2	6	76.2	90
4	2	7.2	78.8	100.0
5	4	2	49	60
6	4	4	48.7	52.6
7	4	6	54.8	65.5
8	4	7.2	54.4	62.1
9	6	2	51.8	58.1
10	6	4	48.2	52.9
11	6	6	54.4	58.3
12	6	7.2	52.5	55.6

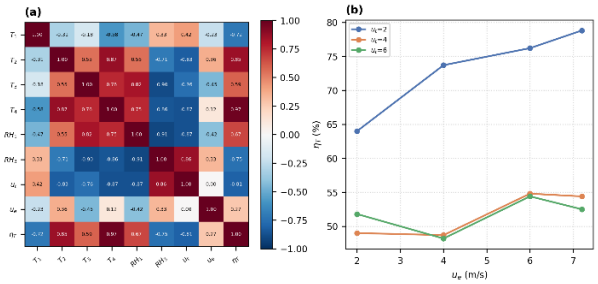


Figure 5. (a) Pearson correlation matrix; (b) effect of u_t on T_4 and η_T by u_t level.

5.4 Correlation Analysis and Efficiency Comparison

Table 3 compares η_T (Equation (3)) and η_{K203} (Equation (4)). As expected, η_{K203} consistently exceeds η_T because its denominator (T_1 -T_2) is smaller than (T_1 -T_3); Spearman rank correlation between the two metrics equals 1.00.

Figure 5 presents the Pearson correlation matrix (panel a) and the velocity effect on T_4 by u_t level (panel b). The strong negative correlation $r(u_t, \eta_T) \approx -0.81$ ($p < 0.01$) and weak positive $r(u_e, \eta_T) \approx +0.27$ ($p < 0.10$) are statistically consistent with the velocity analysis.

5.5. Energy Efficiency and Carbon Reduction

Figure 6 quantifies the environmental impact of passive HRV operation. Recovered power spans 245-713W (panel a, Equation (6)). The highest absolute power occurs at u_t=6 m/s (large mass flow) despite lower η_T, demonstrating that power and efficiency are non-equivalent optimization objectives. A two-sided energy balance was also evaluated. With the corrected supply mass flow (d=0.15 m), the supply-side gain $\dot{M}=\dot{m}_t \cdot c_p \cdot (T_4-T_3)$ spans 245-713 W, whereas the exhaust-side release $\dot{m}e \cdot cp \cdot (T_1-T_2)$ spans only 104-497 W; the two sides do not close (supply/exhaust ratio 1.0-3.8, largest at high ut and low ue).

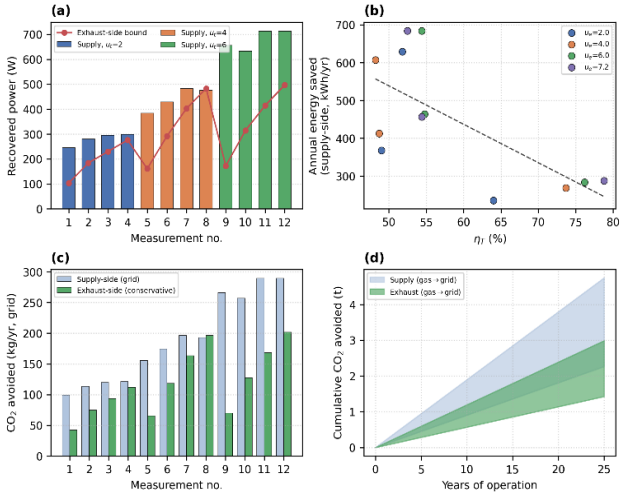


Figure 6. Two-sided energy and carbon analysis. (a) Recovered power: supply-side bars (by u_t) with the exhaust-side release as the recovery bound; (b) annual supply-side energy saving vs. η_T; (c) annual CO_2 avoided (grid factor), supply-side vs. conservative exhaust-side; (d) cumulative 25-year CO_2 avoided for the mean unit, each band spanning the natural-gas→grid emission factors.

Since the heater is off, the excess supply-side heat can only originate from the ≈ 21°C ambient surrounding the unit, i.e. parasitic casing gain. The exhaust-side release is therefore taken as the defensible upper bound on genuine air-to-air recovery, giving conservative annual savings of 99-477 kWh/year and CO_2 avoidance of 20-96 kg (natural gas) or 42-202 kg (grid electricity) per unit.

From Equations (7) and (8), annual energy savings reach 236-685 kWh/year and CO_2 avoidance 48-138 kg/year (natural gas) or 100-290 kg/year (grid electricity) per unit (panels b-c). Over a 25-year service life (panel d), the mean unit avoids 2.3–4.7 tCO_2 on the supply-side estimate and 1.4–3.0 tCO_2 on the conservative exhaust-side basis (natural-gas to grid factors), i.e. meaningful contributions at campus or district scale with multiple units [27].

6. Conclusion

This study presented an integrated experimental and ML based analysis of the Argemsan K-203 cross-flow plate HRV system in fully passive mode (heater off) under real winter conditions (outdoor 7.8°C /81%RH, indoor 21.1°C/55%RH). Key findings:

- Passive heat recovery raised T_4 to 15.1-18.3°C from outdoor 9.4-11.3°C with zero auxiliary energy.
- η_T : 48.2-78.8% (mean 58.9%); η_{RH}: 59.0-98.0% on a relative-humidity basis (mean 75.7%), corresponding to 35-59% (mean 44%) latent effectiveness when evaluated on the humidity ratio.
- u_t is the dominant control variable: increasing u_t from 2 to 6 m/s reduced η_T by up to 25 pp. Minimizing u_t within ventilation constraints is the highest-leverage control action.
- RF: R^2 = 0.931, MAE= 0.261°C for T_4. GB: R^2=0.880 for η_T. Minimal sensor set {T_1, T_3, u_e} is not supported; the importance analysis instead identifies the supply velocity and inlet humidities as the dominant inputs, so

sensor reduction remains future work.

- Optimal band: $u_t = 2$ m/s, $u_e \geq 6$ m/s ($\eta_T \approx 60.1\%$, This surrogate optimum (≈60.1%) lies below the best directly measured value (78.8% at ut=2 m/s, ue=7.2 m/s) because the surface is evaluated at the mean inlet temperature T3=9.9°C, whereas the highest-efficiency points coincided with a warmer inlet (T3≈10.5°C). The response surface should therefore be interpreted as an interpolation at mean conditions, not as an attainable global optimum.$T_4 \approx 16.5$°C).
- 236–685 kWh/year and 48-138 (gas)/100-290 (grid) on the supply side, and conservatively 20-96/42-202 on the exhaust-side balance kgCO_2/year per unit; 2.3–4.7 tCO_2 (supply) or 1.4–3.0 tCO_2 (conservative exhaust) over 25 years.

These findings should be read as an exploratory, single-unit characterization rather than a generalizable predictive framework. With only 12 active operating points, the machine-learning models are used descriptively; the reported R2 values carry wide sampling uncertainty, and the response-surface, optimal-band, and sensor-reduction statements are first-order indications that require confirmation on larger, replicated, and multi-climate datasets.

Future work should extend to larger seasonal datasets, transient inertia modelling, and deployment of the RF response surface (Figure 4) as a surrogate within a model-predictive controller.

Declaration

The author declared no potential conflicts of interest with respect to the research, authorship, and/or publication of this article. The author also declared that this article is original, was prepared in accordance with international publication and research ethics, and ethical committee permission or any special permission is not required. All figures in this article are original and were produced by the author; none have been reproduced from third-party sources, and therefore no copyright permissions are required.

This work advances energy-efficient passive ventilation and supports building decarbonization. No foreseeable negative societal consequences are anticipated.

Author Contribution

Hakan Tutumlu: Conceptualization, Methodology, Experimentation, Data curation, Formal analysis, Software, Visualization, Writing – original draft, and Writing – review & editing. The sole author read and approved the final manuscript.

References

1. International Energy Agency, *Buildings – Tracking Clean Energy Progress*. IEA, Paris, France, 2022.
2. European Parliament and Council of the European Union, *Directive (EU) 2018/844 of the European Parliament and of the Council of 30 May 2018 amending Directive 2010/31/EU on the energy performance of buildings and Directive 2012/27/EU on energy efficiency*. Official Journal of the European Union, 2018. **L156**: p. 75–91.
3. Aridi, R., et al., *Energy recovery in air conditioning systems: Comprehensive review, classifications, critical analysis, and potential recommendations*. Energies, 2021. **14**(18): p. 5869.
4. European Committee for Standardization (CEN), *EN 308:1997 – Heat exchangers: Test procedures for establishing the performance of air to air and flue gases heat recovery devices*. European Committee for Standardization, Brussels, Belgium, 1997.
5. Choi, Y.H., et al., *Analysis of the variable heat exchange efficiency of heat recovery ventilators and the associated heating energy demand*. Energy and Buildings, 2018. **172**: p. 152–158.
6. Nasif, M., et al., *Membrane heat exchanger in HVAC energy recovery systems, systems energy analysis*. Energy and Buildings, 2010. **42**(10): p. 1833–1840.
7. Aste, N., M. Manfren, and G. Marenzi, *Building Automation and Control Systems and performance optimization: A framework for analysis*. Renewable and Sustainable Energy Reviews, 2017. **75**: p. 313–330.
8. Aghili, S.A., et al., *Artificial intelligence approaches to energy management in HVAC systems: A systematic review*. Buildings, 2025. **15**(7): p. 1008.
9. Breiman, L., *Random forests*. Machine Learning, 2001. **45**(1): p. 5–32.
10. Argemsan Eğitim Teknolojileri San. ve Tic. A.Ş., *K-203 Geri Isı Kazanımlı Lokal Havalandırma Eğitim Seti – Kullanım Kılavuzu*. Balıkesir, Türkiye, 2025.
11. Fanger, P.O., *Thermal Comfort: Analysis and Applications in Environmental Engineering*. Danish Technical Press, Copenhagen, Denmark, 1970. p. 244.
12. Persily, A.K. and S.J. Emmerich, *Indoor air quality in sustainable, energy efficient buildings*. HVAC&R Research, 2012. **18**(1–2): p. 4–20.
13. Persily, A.K., *Field measurement of ventilation rates*. Indoor Air, 2016. **26**(1): p. 97–111.
14. Zhao, L. and J. Liu, *Physical environmental and behavioral drivers of heat recovery ventilation system feasibility in various climate zones*. Energy Conversion and Management, 2022. **259**: p. 115586.
15. Elmacıoğlu, H.Ü., et al., *Analysis and design of an air to air heat exchanger used in energy recovery systems*. Journal of Energy Systems, 2022. **6**(1): p. 108–130.
16. Moro, A. and P. Kwakye-Boateng, *Heat recovery analysis of a fixed plate energy recovery ventilator*. Sustainable Energy Research, 2024. **11**: p. 29.
17. Moghadam, T.T., et al., *Energy efficient achievement of indoor air quality and thermal comfort using mechanical ventilation heat recovery and solar-energy pre-heating*. Energy Conversion and Management, 2025. **327**: p. 119528.
18. Kılıç, M., et al., *Increasing the thermal performance of cooling tower by utilizing swirling jets*. International Advanced Researches and Engineering Journal, 2020. **4**(2): p. 57–63.
19. Hamburg, A., et al., *Ventilation strategies for deep energy renovations of high-rise apartment buildings: Energy*

efficiency and implementation challenges. Energies, 2025. **18**(11): p. 2785.

20. Amir, F., et al., *Performance analysis of heat recovery in Heat Pipe Heat Exchanger on room air conditioning systems*. AIMS Energy, 2023. **11**(4): p. 612–627.
21. Tsanas, A. and A. Xifara, *Accurate quantitative estimation of energy performance of residential buildings using statistical machine learning tools*. Energy and Buildings, 2012. **49**: p. 560–567.
22. Kallio, J., et al., *Forecasting office indoor CO2 concentration using machine learning with a one-year dataset*. Building and Environment, 2021. **187**: p. 107409.
23. Demirezen, G., A.S. Fung, and M. Deprez, *Development and optimization of artificial neural network algorithms for the prediction of building specific local temperature for HVAC control*. International Journal of Energy Research, 2020. **44**(11): p. 8513–8531.
24. Wang, H., et al., *A review of deep learning for renewable energy forecasting*. Energy Conversion and Management, 2019. **198**: p. 111799.
25. International Energy Agency, *CO2 Emissions in 2022*. IEA, Paris, France, 2023.
26. Intergovernmental Panel on Climate Change (IPCC), *2006 IPCC Guidelines for National Greenhouse Gas Inventories, Volume 2: Energy*. Institute for Global Environmental Strategies, Hayama, Japan, 2006.
27. Bao, L., J. Wang, and H. Yang, *Investigation on the performance of a heat recovery ventilator in different climate regions in China*. Energy, 2016. **104**: p. 85–98.
28. Menter, F.R., M. Kuntz, and R. Langtry, *Ten years of industrial experience with the SST turbulence model*, in *Turbulence, heat and mass transfer*. 2003. **4**(1): p. 625-632.
29. Bühlmann, P. and B. Yu, *Analyzing bagging*. The Annals of Statistics, 2002. **30**(4): p. 927–961.
30. Friedman, J.H., *Greedy function approximation: A gradient boosting machine*. The Annals of Statistics, 2001. **29**(5): p. 1189–1232.
31. Friedman, J.H., *Stochastic gradient boosting*. Computational Statistics & Data Analysis, 2002. **38**(4): p. 367–378.
32. Friedman, J., T. Hastie, and R. Tibshirani, *Additive logistic regression: A statistical view of boosting*. The Annals of Statistics, 2000. **28**(2): p. 337–407.
33. Hastie, T., R. Tibshirani, and J. Friedman, *The Elements of Statistical Learning: Data Mining, Inference, and Prediction*. 2nd ed. Springer, New York, USA, 2009.
34. Dietterich, T.G., *Ensemble methods in machine learning*, in *International workshop on multiple classifier systems*. Springer, Berlin, Heidelberg, 2000. p. 1-15.
35. Durap, A., *Machine learning-based wind speed prediction using random forest: A cross-validated analysis for renewable energy applications*. Turkish Journal of Engineering, 2025. **9**(3): p. 508–518.
36. İzgi, B., *Machine learning predictions and optimization for thermal energy storage in cylindrical encapsulated phase change material*. International Journal of Energy Studies, 2024. **9**(2): p. 199–218.